

Water-induced crystallization and nano-scale spinodal decomposition of cellulose in NMMO and ionic liquid dope

Yoshiharu Nishiyama, Shirin Asaadi, Patrik Ahvenainen, Herbert Sixta

▶ **To cite this version:**

Yoshiharu Nishiyama, Shirin Asaadi, Patrik Ahvenainen, Herbert Sixta. Water-induced crystallization and nano-scale spinodal decomposition of cellulose in NMMO and ionic liquid dope. Cellulose, 2019, 26 (1), pp.281-289. 10.1007/s10570-018-2148-x . hal-02390952

HAL Id: hal-02390952
https://hal.science/hal-02390952

Submitted on 6 Aug 2022

HAL is a multi-disciplinary open access archive for the deposit and dissemination of scientific research documents, whether they are published or not. The documents may come from teaching and research institutions in France or abroad, or from public or private research centers.

L'archive ouverte pluridisciplinaire **HAL**, est destinée au dépôt et à la diffusion de documents scientifiques de niveau recherche, publiés ou non, émanant des établissements d'enseignement et de recherche français ou étrangers, des laboratoires publics ou privés.

Water-induced crystallization and nano-scale spinodal decomposition of cellulose in NMMO and ionic liquid dope

Yoshiharu Nishiyama[1]*, Shirin Asaadi[2], Patrik Ahvenainen[3], and Herbert Sixta[2]

[1] *Univ. Grenoble Alpes, CNRS, CERMAV, 38000 Grenoble, France*

[2] *Department of Bioproducts and Biosystems, Aalto University, P.O. Box 16300, Vuorimiehentie 1, Espoo, FI-00076, Finland*

[3] *Department of Physics, University of Helsinki, P.O. Box 64, FI-00014, Finland*

Phone: +33 (0) 476 03 76 05

E-mail: yoshi@cermav.cnrs.fr

We followed the cellulose structure formation induced by water diffusion into Lyocell dopes based on both N-Methylmorpholine N-oxide (NMMO) and 1,5-diazabicyclo[4.3.0]non-5-ene acetate ([DBNH][OAc], by using scanning simultaneous small- and wide-angle scattering (SAXS-WAXS) experiment along the diffusion gradient. The water content at each point was estimated from the wide-angle scattering profile, giving a binary diffusion constant of the order of 5×10^{-10} m^2/sec. In the case of the cellulose solution in NMMO monohydrate, diffraction peaks corresponding to cellulose II appeared concomitantly with the increase in small angle scattering features indicative of nanofibril formation. In the cellulose solution in the ionic liquid, an increase in small angle scattering intensity with the progression of water content appeared at scattering vector q = 0.015 $Å^{-1}$ corresponding to a correlation length of about 40 nm, indicative of nanometric spinodal decomposition preceding the coagulation process, though no crystalline peak appeared in the wide-angle scattering.

SAXS-WAXS, dissolution, regeneration, coagulation, diffusion, ionic liquid

Introduction

Structure formation during the processing from highly concentrated solution dope is a crucial step in controlling the final material properties in solution processing, including fiber spinning, membrane generation or fabrication of other functional materials. One of the reasons for the success of viscose process for the manufacture of regenerated cellulose fibers, despite its environmental concerns, is its ability to adjust various fiber properties and supramolecular structures by modifying the operational conditions. For other potential solvent systems that can be more environmentally benign to be deployed more massively, the control of the structural formation is a key. However, little is known on the structure formation process at nanoscale. NMMO is a solvent used in the industrial production of cellulose fibers called Lyocell while [DBNH][OAc] is a new ionic solvent that has promising characteristics as next generation solvent for cellulose processing (Sixta2015). Both are miscible with water but lose their cellulose dissolution capacity with excess water. Thus water is used as non-solvent to regenerate cellulose. In the spinning process, the humidity in the air gap is known to be an important parameter (Mortimer1996), but its role remains hypothetical in the absence of experimental data on the structure modification.

The regeneration of cellulose by a non-solvent, in this case water, is a complex process involving diffusion of non-solvent into the dope, diffusion of different solvent molecules into coagulation bath and the structure formation and swelling or contraction of the regenerating gel. Thus there is a huge difference in estimated diffusion coefficients depending on the experimental approach and the diffusion model employed.

A critical review of the literature data is available in a recent report by Hedlund et al (2017). The reported value of diffusion coefficient of water and NMMO in NMMO/cellulose dope measured by visual inspection of diffusion front (Biganska2005), after correction of equation as pointed out by Hedlund et al (multiplication by factor of 4), was 4.4×10^{-9} m^2/s, which is higher than the self-diffusion coefficient of water at ambient conditions (2.57×10^{-9} m^2/s). The self-diffusion of NMMO to the coagulation bath was estimated to be about one order of magnitude lower, and further decreasing in the presence of cellulose (Biganska2005).

By using NMR diffusometry, Laity et al (2012) assessed the self-diffusion coefficient of NMMO and water molecules in NMMO/cellulose solution to be of the order of 4×10^{-12} m^2/s, which increases to the order of 1.5×10^{-9} m^2/s in the course of coagulation with water, while effective mutual diffusion during coagulation as estimated from composition change was 1.4×10^{-10} m^2/s with the NMMO loss and water influx to be identical (Laity2002). Similar NMR studies on ionic liquid systems show the diffusion coefficient of pure ionic liquid (1- ethyl-3-methyl-imidazolium acetate) to be 10^{-11} m^2/s and this value can go down by two orders of magnitude in the presence of carbohydrates due to the association with hydroxyl groups (Ries 2014). In the ionic liquid-water system, the diffusion constant of ionic liquid increases under the presence of water, while that of water is slowed down by the presence of an ionic liquid (Hall2012).

The diffusion of solvents and non-solvents during the regeneration of cellulose depend also on the network structure of regenerating cellulose. Gavillon and Budtova (2007) measured decreased

diffusion coefficients of NaOH and NMMO in the presence of coagulating cellulose that would indicate homogeneous gel formation where individual chains would interact with the solvent.. On the other hand Hedlund (2017) observed little effect of cellulose in [C2min][OAc] system indicative of heterogeneous gel formation in which most of cellulose chains would be excluded from the solvent system.

However, diffusion is also affected by many factors such as intermolecular interactions. The structure of coagulating cellulose, which can also depend on the cellulose concentration, cannot be directly determined from the diffusion data alone. X-ray scattering is a powerful tool to probe the spatial arrangement, from sub-nanometric to sub-micrometric length scale inside a sample. In this study, we measured simultaneous small- and wide-angle X-ray scattering on regenerating cellulose near water (coagulant) solution interface to follow the structural formation.

Experimental

Materials

Birch pre-hydrolyzed kraft pulp (PHK) with DP 1007, Mw = 274.3 kg mol^{-1} , Mn = 68.2 kg mol^{-1} and PDI = 4 from Stora Enso Enocell Mill, Finland was used as a cellulose solute. 1,5-Diazabicyclo[4.3.0]non-5-ene (DBN) (99%, Fluorochem, UK) and glacial acetic acid (Merck, Germany) were used as received. [DBNH][OAc] ionic liquid was synthesized by slowly adding equimolar amounts of acetic acid to DBN under cooling (Michud 2015). The cellulose solutions were prepared in a 200 ml vertical kneader rotating at 30 rpm, under a vacuum of 3 to 5 mbar. The temperature was regulated to 90°C for the NMMO system and 80˚C for [DBNH][OAc] system. It took 90 minutes to prepare a 10 wt% cellulose solution. For the NMMO system, 0.15 to 0.28 g of propyl gallate was added to the dopes as stabilizer.

The samples were put in a glass tube with an outer diameter of 3 mm and a wall thickness of 200 µm. The [DBNH][OAc] cellulose solution was viscoelastic at room temperature, and thus a hot solution was centrifuged at 3000 rpm for 1 min to fill in the bottom of the tube. The cellulose-NMMO dopes were solid at room temperature, and could be easily loaded into the tubes.

X-ray scattering

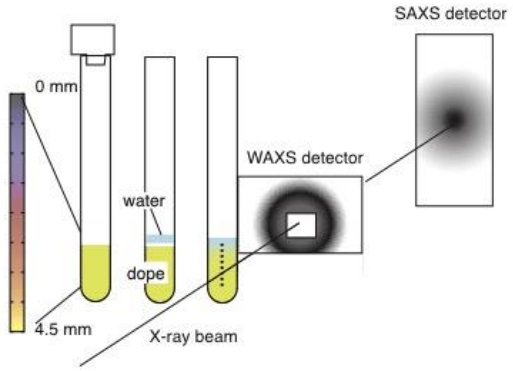


Figure 1. Schematic illustration of the experimental setup.

The X-ray scattering experiment was carried out at the D2AM beamline of the ESRF. Two silicon pixel detectors were used simultaneously. A detector with central hole, "WOS" (imXPAD, France) was placed at about 7 cm from the sample and a rectangular detector "XPAD-D5" (imXPAD, France) was placed at 1.5 m from the sample. The sample tubes were mounted on a temperature controlled sample exchanger with 3 mm diameter holes mounted on a motorized sample stage. X-ray energy of 18 keV ($\lambda = 0.689$ Å) was chosen to limit the attenuation by the glass tube. The exposure time was 10 seconds for each frame. The incident and the transmitted beam intensities were monitored by scintillation counters placed before and behind the sample respectively. The scattered intensity was normalized with respect to the transmitted intensity, and the scattering signal from the empty glass tube was subtracted. The intensities were circularly averaged after Lorentz-polarization correction using an inhouse software, and converted to differential scattering cross sections [cm^{-1}] by calibrating with water scattering intensity (Dreiss2006). The scattering intensities are presented as a function of the magnitude of the scattering vector

$$q = \frac{4\pi \sin\theta}{\lambda} (\text{Å}^{-1})$$

where 2θ is the angle between the incident beam and the scattering direction.

Wide angle scattering of solvent and water content

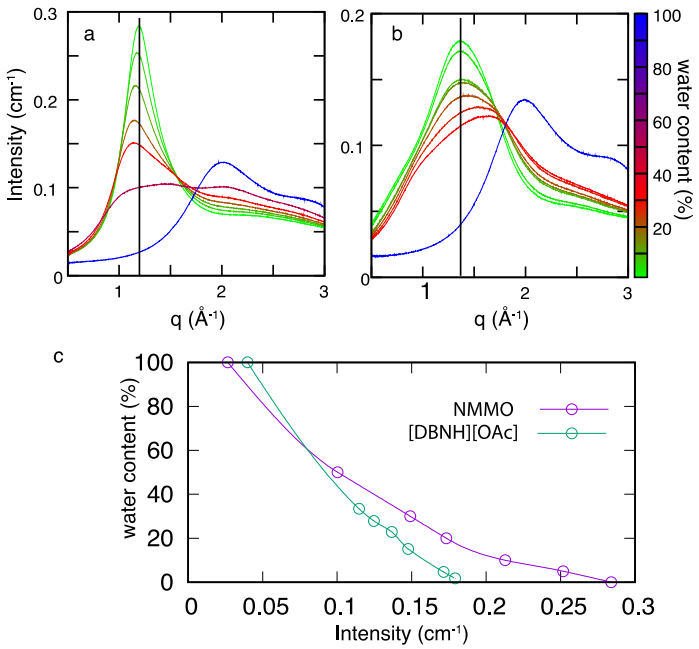


Figure 2. Wide angle scattering of solvent-water mixture of (a) NMMO monohydrate at 90˚C and (b) [DBNH][OAc] at 80˚C as a function of water content (not taking into account the initial hydration of NMMO). c: Relationship between water content and the scattering intensity at 1.2 $Å^{-1}$

for NMMO monohydrate and 1.4 $Å^{-1}$ for [DBNH][OAc]. Data points were connected with an Akima spline interpolation (solid line in the figure)

A series of X-ray scattering profiles of solvent-water mixtures measured at 80˚C for [DBNH][OAc] and 90˚ C for NMMO monohydrate are presented in figure 2. The scattering of neat [DBNH][OAc] and NMMO monohydrate has maximum intensity at q = 1.4 and 1.2 $Å^{-1}$ respectively whereas water scattering peaks at around 2 $Å^{-1}$. With increasing water content, the scattering profile continuously changes and each mixture has a unique profile. The relation between water content and intensity at these peak positions are plotted in figure 2c, where a reasonable estimate of water content can be obtained from the single intensity value. An Akima spline (Akima1970) was used to relate the intensity to the water content. In the case of cellulose dope, the presence of cellulose would slightly modify the wide angle scattering, but this effect was neglected as a first approximation.

In-situ monitoring of coagulation

To follow the coagulation process with contact to water, the sample was filled to approximately 5 mm from the bottom of the tube, mounted on the temperature controlled sample holder, and a water drop (ambient temperature) was inserted from the top to allow diffusion into the solution. The temperature was maintained at 80˚C for the [DBNH][OAc] system and 90˚C for the NMMO system. The sample was vertically scanned before and after addition of water and with regular interval to monitor the structural evolution.

Results and discussions

Water diffusion from wide angle scattering

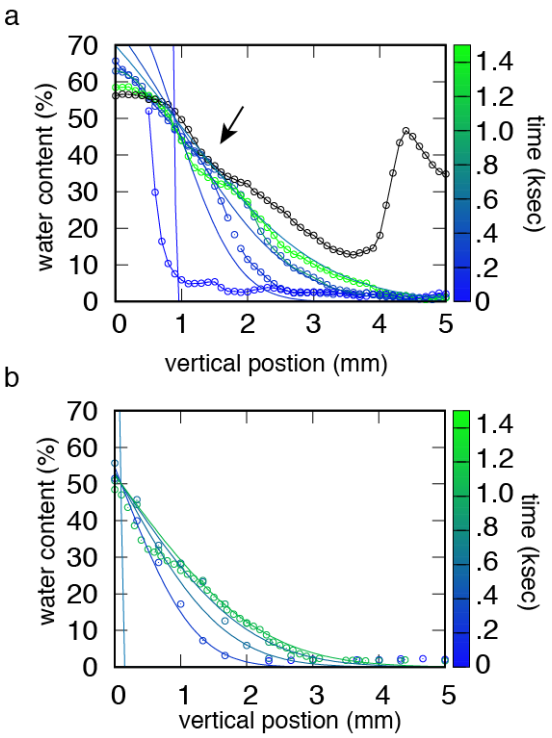


Figure 3. Water contents as function of position during regeneration from (a) NMMO and (b) [DBNH][OAc] as calculated from the scattering intensity at q = 1.2 $Å^{-1}$ for NMMO and q = 1.4 $Å^{-1}$ for [DBNH][OAc] according to Fig 2c. The black curve in (a) is obtained after cooling at room temperature. The apparent steps in (a) are probably an artifact due to the crystallization as seen in figure 4.

When water is added the wide-angle scattering feature reproduces the scattering features of water-NMMO mixture and water-[DBNH][OAc] mixture with increasing concentration of water towards the top of the tube. The water content estimated from the scattering intensity at q = 1.2$Å^{-1}$ and at q = 1.4 $Å^{-1}$ according to Fig 2c as a function of vertical position is plotted in figure 3. For a Fickian diffusion with a constant diffusion constant *D*, the water content *C* at position *x* from the interface, after time *t* since the contact with water can be expressed as (Crank1975)

$$C(x,t) = \text{erfc}\,(x/(4tD)^{1/2})$$

This prediction of concentration distribution is overlapped as solid line on the concentration evaluated from the scattering intensity. Here, in both cases, a mutual diffusion constant of 5×10^{-9} m^2/s was used. Since the volume beneath the vertical reference position is held constant by the tube wall, the influx of water into the solution is equal to the solvent and cellulose outflux from vertical position 0. The self-diffusion coefficient of water at 80˚C is 6.25×10^{-9} m^2/s (Yoshida2008) so the apparent diffusion coefficient is not far from the pure water, contrary to what was estimated

from NMR diffusometry. In some places the water diffusion seems to be even faster (arrow in fig. 3) which might be due to the presence of microcavities.

Regeneration from NMMO solution

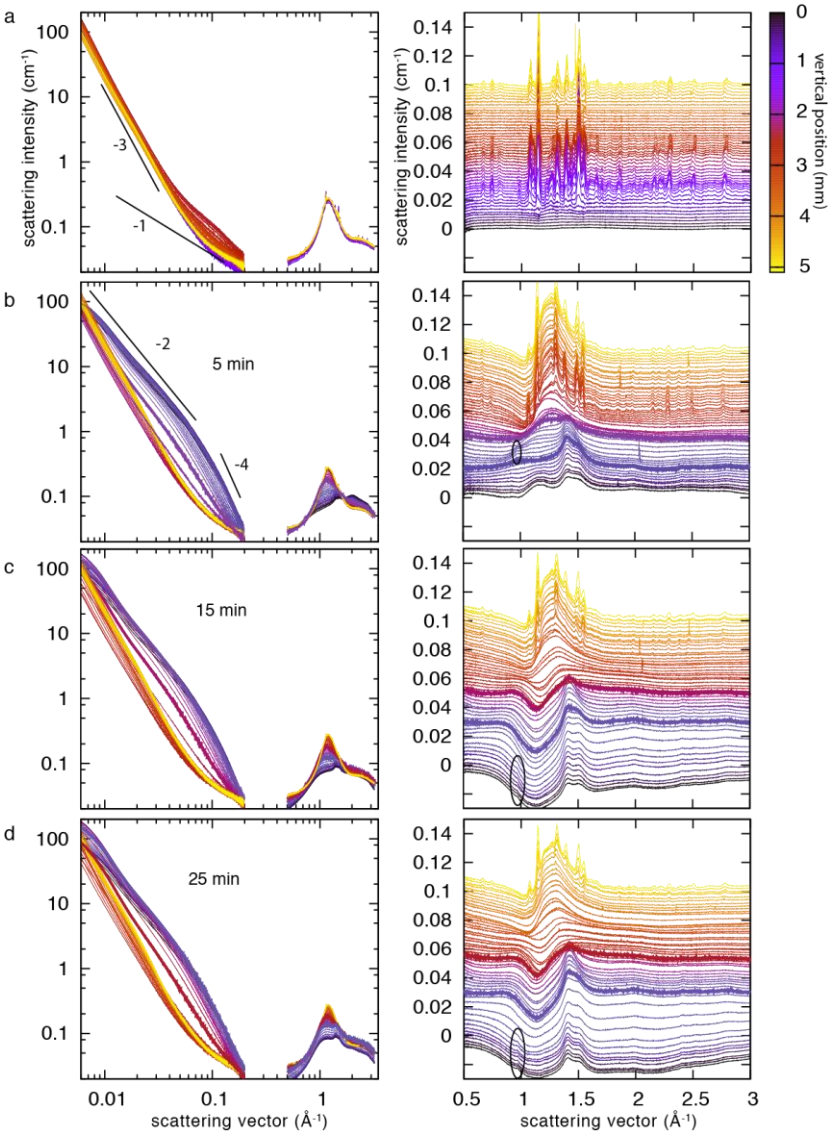


Figure 4 a-d: Small- and wide-angle X-ray scattering profiles of 10% cellulose dope in NMMO monohydrate as a function of vertical position along the tube (color code) at 90˚C before addition of water (a) and 5 min (b), 15 min (c) and 25 min (d) after addition of water. The left figures are double logarithmic plots of data covering both wide- and small angle scattering data, and the right figures are linear scale plots after subtraction of solvent/water mixture profile obtained by interpolation of experimental data in Figure 2, with water content estimated from the scattering intensity at q = 1.2 ($Å^{-1}$) according to figure 2c. The profiles at the transition when the peak appears at q = 1.4 and 1.5 $Å^{-1}$ are drawn with thicker lines for clarity. Power law lines with different exponents are indicated as guides to the eye.

Before the addition of water, the small-angle scattering of cellulose solution in NMMO monohydrate at 90˚C followed a power law with an exponent of -3 below q = 0.08 $Å^{-1}$, steeper than what would be expected for an extended polymer chain segments. This excess scattering intensity below q = 0.08 $Å^{-1}$ indicates heterogeneity of the solution structure or density fluctuations at least at a nanometric length scale. In the wide-angle range, depending on the position of the beam, sharp crystalline peaks can be seen (figure 4a right). On the other hand the feature in the small angle region below q = 0.04 $Å^{-1}$ is independent of position, and thus should not be related to the crystallization seen in the wide-angle scattering that is more heterogeneous and localized. One possibility would be micro cavities with irregular surfaces or polydisperse nanobubbles created during the crystallization of NMMO when the solution was cooled down. In theory, the high surface tension could lead to rapid Ostwald ripening. The kinetics of Ostwald ripening also depends on the volume fraction of bubbles and the solubility of the gas, which can be small. The intensity increase at low q can also be due to the aggregation of cellulose chains. In this case, it would be a loose association of cellulose chains as there is no sign of cellulose crystallinity in the wide-angle scattering. Some positions show a shoulder appearing at around q = 0.1 $Å^{-1}$, which again does not correlate with crystalline peak intensity. For the moment we do not have any explanation for this feature.

In the small-angle region, about five minutes after the addition of water (Fig. 4b), the scattering intensity in the q-range of 0.01 - 0.02 $Å^{-1}$ increases at positions close to the water interface, up to vertical position of 2 mm, due to a coarse structuring (thick line in fig 4b). On the other hand, the intensity decreased in lower positions with diffusion of water. This decrease can be explained if the scattering from the dope originated from microcavities that are now filled with water in the first place, thus reducing the electron density contrast between the cavity and the bulk.

The first increase in intensity from the original profile can be seen between q = 0.03- 0.1 $Å^{-1}$ at a position 2 mm from the top, corresponding to about 10 wt-% water content (not counting the hydration molecule of the monohydrate). The exact peak position of the new signal cannot be determined due to the uncertainty of the high scattering coming from the coarse structure that exist already before addition of water.

In the wide-angle range, the sharp diffraction disappears at water content of about 5% (vertical position = 2.5 mm), and a crystalline peak typical of polymer crystals starts to appear at the vertical position of 2 mm, corresponding to a water content of 10%, first at q = 1.4 $Å^{-1}$ followed by another peak at q = 1.5 $Å^{-1}$ further closer to the interface (v. p. = 1.8 mm, water content =15%, drawn with thick line in fig. 4b). These peaks corresponds to a d-spacings of 4.5 and 4.2 Å respectively which is close to the strongest reflections of cellulose II, 1 1 0 and 0 2 0 (d = 4.4 and 4.0 Å), and is probably due to the crystallization of cellulose essentially in the direction perpendicular to the pyranose plane, and not completely in form of cellulose II, as the peak positions are slightly different and 1-10 cannot be seen. The two peaks are also quite similar to Na-cellulose complex (Nishiyama2000), and might be due to a similar loose complex structure involving NMMO molecules. The very early stage of coagulation showing only one peak at d = 4.5 Å is also reported by Fink et al (2001) in the never-dried fiber from the NMMO system. In our

condition the crystalline order grew perpendicular to the hydrophobic stacking as well, though to a smaller size than in the hydrophobic stacking direction.

The scans at 15 and 25 minutes after the introduction of water (Fig. 4c, d) capture the progression of water diffusion and the accompanying structure formation. In both cases, the change in small-angle scattering features coincided with the appearance of the first diffraction peak at q = 1.4 $Å^{-1}$, indicating that the structuration is essentially due to crystallization, or stacking of chains in one direction occurring at relatively low water content of 10%.

Some aspects seem to be governed by timescale accessible in this experiment ~ minutes. For example, a small peak at 0.97 $Å^{-1}$ corresponding to d = 6.5 Å first appears after 5 min in the zone where water content is 30-40%, but disappears from this zone in the later stages, reappearing in the zone closer to the water interface. The current data do not allow a clear molecular view of the structure formation, but the distance would be compatible with molecular distances in the plane parallel to pyranose plane.

The slope of the small angle scattering between q = 0.1 and 0.2 $Å^{-1}$ is close to -4 and is compatible with formation of nanometric crystalline fibrils that make clear boundaries between the solvent, Between q=0.01 and 0.06 $Å^{-1}$, the slope is close to -2, typical of a flat object. The diffraction features suggested that the crystallization to be very directional, perpendicular to the pyranose plane, which agrees with the vision of a flat ribbon to be formed. For comparison, figure 5 shows a simulated scattering profile for a randomly oriented cuboid 200 nm long, 40 nm wide and with thickness ranging from 2 to 8 nm, which show general agreement with the scattering profile, especially when the thickness was 2 nm. A thickness of 2 nm could correspond to about three layers of cellulose sheets intercalating NMMO and water molecules. At q above 0.2 $Å^{-1}$, the simulation deviates from the observation, as the coagulated object cannot be considered as homogeneous cuboid at this length scale giving rise to excess scattering in the real world. Of course this is not the only model that can explain the small small-angle scattering profile and it should be considered as one of the plausible models.

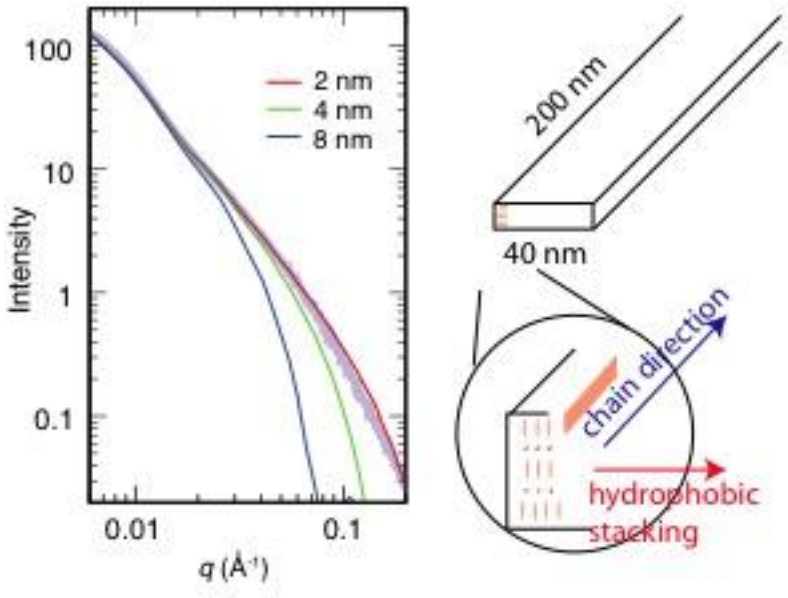


Figure 5. Simulated scattering profile (left) of cuboid presented on the right with different thicknesses (2, 4, 8 nm) overlapped with the experimental data from Fig 4d (thick lines) showing good agreement with the 2 nm thick model .

Regeneration from [DBNH][OAc] solution

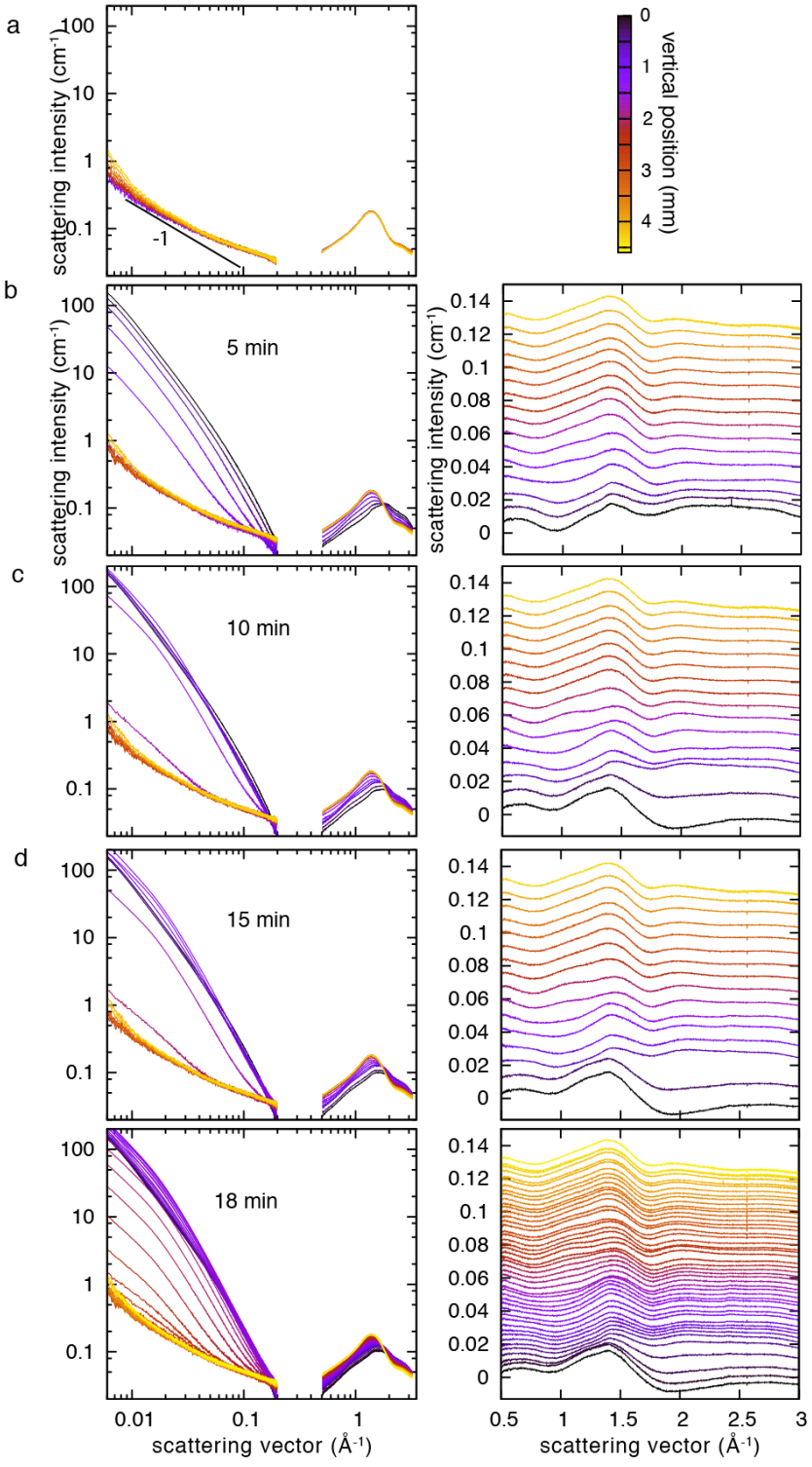


Figure 6. Small- and wide-angle X-ray scattering profiles of 10% cellulose dope in [DBNH][OAc] as a function of vertical position along the tube (color code) at 80˚C before addition of water (a) and 5 min (b), 10 min (c) 15 min (d) and 18 min (e) after the addition of water

X-ray scattering profiles of 10% cellulose solution in [DBNH][OAc] at 80˚C is shown in figure 6a. Contrary to NMMO solution, there is no indication of a coarse structure or density fluctuation except for slight excess intensity at lowest q ~ 0.01 $Å^{-1}$ in some parts of the sample. The intensity follows $I \sim q^{-1}$ with a prefactor similar to the case of cellulose solution in NMMO monohydrate, typical of a rod-like scattering object.

When water is added, the intensity drastically rises below q = 0.1 $Å^{-1}$ forming concave upward profiles, even with the slightest change in the wide-angle scattering. Throughout the experiment no crystalline peak appeared in the wide-angle scattering. The first event of regeneration is the density fluctuation, probably induced by the spinodal decomposition. This is different from the case of regeneration from NMMO solution where elongated plate-like crystalline domain forms. The regeneration event starts with an appearance of a small shoulder peak in the small angle region between 0.01 and 0.02 $Å^{-1}$ corresponding to a density fluctuation with a periodicity of 30-60 nm. The increase in small angle intensity occurs at water content of about 5% and completes below 15% water content, the transition corresponding to a depth at about 500 µm as judged from the wide-angle scattering according to figure 2.

The spun fibers from [DBNH][OAc] are known to be crystalline, similar to the NMMO-based Lyocell fibers (Sixta2015, Hummel 2016). In this simple experiment, no extensional flow or shear that would force the alignment of cellulose chains exists. In the spinning process, such strain can facilitate the crystallization. Also, the water content at the interface was only 50%, and still the cations can be strongly bound to the cellulose chains impeding the crystallization. The crystallization in the process might be occurring during the washing stage where the solvent concentration is much lower. Indeed the particularity of the [DBNH][OAc] is the apparent slow diffusion from cellulose gel (Hauru2016) that might be due to strong affinity to cellulose. These points will be investigated in the future by analyzing further the washing stage, and the effect of different strain conditions on the sample during the regeneration.

Conclusion

A simultaneous wide- and small-angle X-ray scattering allowed us to follow the water diffusion during regeneration, crystallization behavior and nano-structure formation of cellulose during regeneration process. Unidirectional crystallization was the first step of coagulation in the NMMO dope /water regeneration, while no crystallization was observed in the regeneration process of [DBNH][OAc], up to a water content of approximately 50%.

Acknowledgements

We thank Dr. Isabelle Morfin, Dr. Nathalie Boudet and Dr. Nils Blanc for assistance at the D2AM beamline, and ESRF for providing beamtimes. PA has received funding from Kone Foundation.

References

Akima H (1970) A new method of interpolation and smooth curve fitting based on local procedures. J.ACM 17, 589-602.

Biganska O, Navard P (2005) Kinetics of precipitation of cellulose from cellulose – NMMO – water solutions. *Biomacromol.* 6, 1948-1953.

Crank J (1975) The mathematics of diffusion. second ed. Clarendon Press, Oxford p.14

Dreiss CA, Jack KS, Parker AP. (2006) On the absolute calibration of bench-top small-angel X-ray scattering instruments: a comparison of different standard methods. J. Appl. Cryst. 39, 32-39.

Fink HP, Weigel P, Purtz HJ, Ganster J. (2001) Structure formation of regenerated cellulose materials from NMMO-solutions. Prog. Polym. Sci. 26, 1473-1524.

Hall CA, Le KA, Rudaz C, Radhi A, Lovell CS., Damion RA., Budtova T, and Ries ME (2012) Macroscopic and microscopic study of 1- ethyl-3-methyl-imidazolium acetate−water mixtures. J. Phys. Chem B 116, 12810−12818.

Hauru LKJ, Hummel M, Nieminen K, Michud A, Sixta H (2016) Cellulose regeneration and spinnability from ionic liquids. Soft Matter 12, 1487-1495.

Hedlund A, Könke T, Theliander H (2017**)** Diffusion of ionic liquid – cellulose solutions during coagulation in water: mass transport and coagulation rate measurements. Macromolecules 50, 8707–8719.

Hummel M, Michud A, Tanttu M, Asaadi S, Ma Y, Hauru LKJ, Parviainen A, King AWT, Kilpelainen I, Sixta H (2016) Ionic liquids for the production of man-made cellulosic fibers - opportunities and challenges. Adv. in Polym. Sci. 271, 133-168.

Laity PR, Glover PM, Hay JN (2002) Composition and phase changes observed by magnetic resonance imaging during non-solvent induced coagulation of cellulose. Polymer 43, 5827-5837.

Liu R and Hu X (2006) Precipication kinetics of cellulose in the Lyocell Spinning Process. Ind. Eng. Chem. Res. 45, 2840-2844.

Michud A, Tanttu M, Asaadi S, Ma Y, Netti E, Käärlainen P, Persson A, Berntsson A, Hummel M Sixta H (2015) Ioncell-F: ionic liquid-based cellulosic textile fibers as an alternative to viscose and Lyocell. Textile Res. J. 86, 543-552

Mortimar SA and Peguy A (1996) The influence of air-gap conditions on the structure formation of lyocell fibers. J. Appl. Polym. Sci. 60, 1747-1756.

Nishiyama Y, Kuga S, Okano T (2000) Mechanism of mercerization revealed by X-ray diffraction. J. Wood Sci. 46, 452-457.

Sixta H, Michud A, Hauru L, Asaadi S, Ma Y, King AWT, Kiplenäinen I, Hummel M (2015) Ioncell-F: A High-strength regenerated cellulose fibre. Nordic Pulp & Paper Res. J. 30, 43-57.

323 Yoshida K, Matubayasi N, Nakahara M (2008) Self-diffusion coefficiens of water and organic
324 solvents at high temperatures along the coexistence curve J. Chem. Phys. 129, 214501
325